Biomacromolecules

pubs.acs.org/Biomac

Article

Sulfasalazine- and Cerium Ion-Loaded Polymersomes with Enhanced RONS Scavenging and Colonic Mucosal Repair Ameliorate Experimental Colitis

Miao Sun,[#] Runkai Lv,[#] Yongjie Sha, Luying Zhu, Jun Cao, Zhiyuan Zhong,* and Fenghua Meng*

Cite This: *Biomacromolecules* 2026, 27, 4734−4746

Read Online

ACCESS | Metrics & More | Article Recommendations | Supporting Information

ABSTRACT: Inflammatory bowel disease (IBD) is a relapsing gastrointestinal disorder depicted by persistent oxidative/nitrosative stress, mucosal barrier disruption, and maladaptive immune activation. Herein, we report that sulfasalazine- and cerium ion-loaded polymersomes (SSZ/Ce-Some) that effectively treat IBD through superior capability of scavenging reactive oxygen and nitrogen species (RONS) and promotion of colonic mucosal repair. SSZ/Ce-Some exhibits potent superoxide dismutase (SOD)-like and catalase (CAT)-like catalytic activities, efficiently scavenges representative ROS, and markedly generates oxygen. Its excellent neutralization of RNS (NO) together with superoxide indicates inhibition of tissue-destructive peroxynitrite. SSZ/Ce-Some inhibits inflammatory macrophages and dendritic cell activation and suppresses pro-inflammatory cytokine secretion. In acute colitis, SSZ/Ce-Some accumulates in inflamed colons, alleviates intestinal inflammation, and preserves epithelial tight junction integrity. Moreover, oral SSZ/Ce-Some in a mucoadhesive hydrogel safely and effectively treats chronic Crohn's disease, with tissue repair and immune regulation. Overall, SSZ/Ce-Some with superior RONS-detoxifying capacity represents a promising therapeutic strategy for IBD treatment.

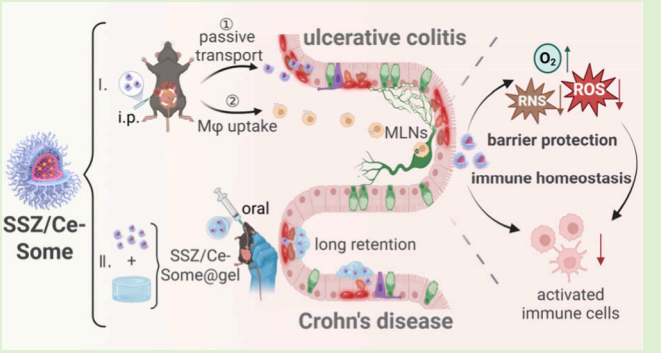

1. INTRODUCTION

Inflammatory bowel diseases (IBDs), including ulcerative colitis (UC) and Crohn's disease (CD), are relapsing inflammatory disorders of the gastrointestinal tract. IBD is characterized by persistent intestinal inflammation, progressive mucosal barrier disruption, immune dysregulation, and an increased risk of colorectal cancer.[1,2] Among current clinical treatments, biologics targeting tumor necrosis factor-α, integrins and interleukin pathways, as well as systemic immunosuppressive therapies, have improved disease control and symptom relief.[3,4] However, biologics require costly repeated injections and risk immunogenicity, while small-molecule drugs suffer from poor absorption, side effects, and high dosing requirements. Moreover, effective mucosal healing or long-term remission remains elusive.

Excessive oxidative stress within the intestinal mucosa has shown to induce epithelial injury, activation of inflammatory pathways, and disruption of redox homeostasis in the gut microenvironment,[5,6] correlating with disease activity in IBD.[7] In parallel, accumulating evidence indicates that nitrosative stress acts as a critical amplifier of tissue injury, while reactive oxygen species (ROS) and reactive nitrogen species (RNS) interact dynamically to form an oxidative−nitrosative network that reinforces immune activation and barrier dysregulation, particularly in chronic disease settings.[8−10] Given this intertwined pathology, modulation of redox imbalance has emerged as a promising adjunctive strategy for IBD treatment.[11,12] Conventional small-molecule antioxidants are, however, rapidly consumed and generally lack catalytic durability and selectivity toward inflammatory sites. Nanomedicines, with advantages in targeted delivery, multimodal therapy, and immune modulation, offer a promising approach for IBD treatment.[13,14] Cerium oxide-based nanozymes, due to the reversible Ce^{3+}/Ce^{4+} redox couple, have demonstrated potent catalytic ROS detoxifying activity and the efficacy in mitigating inflammation.[15,16] However, most redox-active nanotherapeutics developed to date primarily target oxidative stress and are evaluated in acute disease settings. The contribution of nitrosative stress, particularly in chronic intestinal inflammation, remains underexplored.

In this work, we report that sulfasalazine- and cerium ion-loaded polymersomes (SSZ/Ce-Some), which show superior RONS-scavenging ability and colonic mucosal barrier reparative

Received: March 31, 2026
Revised: May 28, 2026
Accepted: June 1, 2026
Published: June 20, 2026

© 2026 American Chemical Society

https://doi.org/10.1021/acs.biomac.6c00702
Biomacromolecules 2026, 27, 4734−4746

Scheme 1. Schematic of the Formation of Sulfasalazine-Integrated Redox-Active Polymersomes (SSZ/Ce-Some) and Enabled Effective ROS/RNS Scavenging, Immune Modulation, And Epithelial Barrier Protection in IBD Models

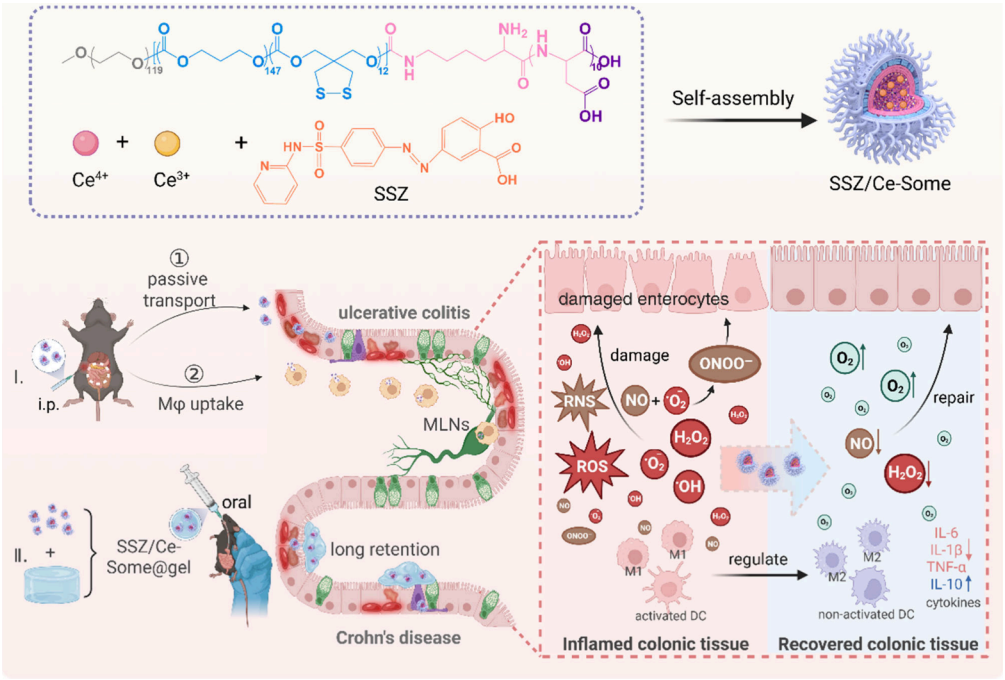

activity, enable effective treatment in both acute and chronic IBD models (Scheme 1). SSZ is a first-line therapeutic for IBD that exerts anti-inflammatory effects by inhibiting cyclo-oxygenase-2 (COX-2) and NF-κB pathways while promoting intestinal mucosal repair,[17,18] though its clinical efficacy is limited by suboptimal bioavailability and poor control of oxidative and nitrosative stress. Interestingly, SSZ/Ce-Some displays potent SOD-like and CAT-like activities with superior ROS and RNS scavenging performance and selective inhibition of inflammatory macrophages. Intraperitoneal administration of SSZ/Ce-Some effectively alleviates acute ulcerative colitis, while oral administration of SSZ/Ce-Some in a mucoadhesive hydrogel (SSZ/Ce-Some@gel) successfully controls chronic Crohn's disease. Therefore, SSZ/Ce-Some, with its combined capability for RONS scavenging and colonic mucosal repair, represents a highly attractive strategy for IBD treatment.

2. EXPERIMENTAL SECTION

2.1. Preparation and Characterization of SSZ/Ce-Some

Take the fabrication of SSZ/Ce-Some with theoretical loading contents of SSZ and Ce at respective 15.7 and 1.7 wt % as an example. Stock solutions A was prepared by dissolving PEG-P(TMC-DTC)-PAsp in DMSO at 80 mg/mL. Sulfasalazine was dissolved in 0.1 mM NaOH at 20 mg/mL and then diluted with HEPES buffer (pH 6.8, 5 mM) to a concentration of 1.5 mg/mL (stock solution B). Then Ce^{3+} and Ce^{4+} mixture (at 3/7 mass ratio, final conc.: 0.14 mg/mL) was blended to 450 μL stock solution B, to which 50 μL solution A was added under mild stirring. After overnight incubation at 37 °C, the obtained SSZ/Ce-Some was subject to purification via dialysis (MWCO: 3500 Da) against HEPES buffer (5 mM, pH 7.4) to obtain self-cross-linked drug-loaded polymersomes. Polymersomes loaded with only SSZ or only Ce ions were prepared (SSZ-Some and Ce-Some) as control using identical method. The size, size distribution, morphology, element compositions, and drug loading were measured using DLS, TEM, elemental mapping, ICP-oes, UV, XPS and XRD. The stability of SSZ/Ce-Some after storage at 4 °C for 6 weeks were investigated by tracking changes in size and size distribution and Ce retention.

2.2. In Vitro ROS Scavenging Experiments

Scavenging capacity of ·OH was assessed using TMB oxidation assay under inflammatory-mimicking condition. Briefly, $FeSO_4$ (1 mM) and H_2O_2 (2 mM) were mixed in sodium acetate buffer (pH 4.5, 0.5 mM), and TMB (25 mM) was added and oxidized to turn a blue color. Then SSZ/Ce-Some, SSZ-Some, Ce-Some, CeNPs (Ce equiv. conc.: 5 μg/mL, SSZ/Ce = 10/1) and PBS were added under stirring, and after 3 min, the absorption at 650 nm was measured by UV−vis (n = 3). Scavenging capacity was calculated based on the absorbance of samples (As) compared to control (Ac, without samples) according to the following formula: $\text{scavenging capacity}(\%) = \left(1 - \frac{\text{As}}{\text{Ab} - \text{As}}\right) \times 100$. For the following experiments, SSZ/Ce-Some was used at Ce conc. of 5 μg/mL (SSZ/Ce = 10/1) if not stated otherwise.

Scavenging capacity of a superoxide anion ($O_2^{\bullet-}$) was evaluated using the WST-8 method. Briefly, WST-8 and xanthine oxidase was mixed to produce a water-soluble formazan, and SSZ/Ce-Some or control samples were added as above (n = 3). After incubation for 30 min, the absorbance at 450 nm was measured, and scavenging capacity was calculated as above.

H_2O_2 scavenging, CAT-like and SOD-like activities of SSZ/Ce-Some were measured using a hydrogen peroxide assay kit, CAT kit and SOD kit according to the manuals, respectively (n = 3). The definition of one CAT activity unit (1 U) is the amount of enzyme that catalyzes the decomposition of 1 μmol of H_2O_2 per minute at 25 °C and pH 7.0. The definition of one SOD activity unit (1 U) is the amount of enzyme that achieves 50% inhibition of the reaction rate in a specific xanthine oxidase-coupled reaction system.

To evaluate intracellular oxygen production capacity, BMDMs were seeded in six-well plates (1×10^5/well) overnight before stimulation with LPS (1 μg/mL) for 12 h. Oxygen probe RDPP and SSZ/Ce-Some were added. After 4 h incubation in the dark at 37 °C, cells were measured using flow cytometry and analyzed using Flowjo (n = 3).

2.3. In Vitro RNS Scavenging Capacity

Intracellular RNS (NO) clearance was assessed by using DAF-FM-DA as a probe. BMDMs seeded in 24-well plates (1×10^5/well) were incubated overnight before LPS stimulation (1 μg/mL) for 12 h. SSZ/Ce-Some or controls were added to incubate for 4 h. Then DAF-FM-

https://doi.org/10.1021/acs.biomac.6c00702
Biomacromolecules 2026, 27, 4734−4746

DA was added and incubated for 30 min at 37 °C in the dark. Cells were imaged using fluorescence microscopy and semiquantified (n = 3).

2.4. In Vitro Cellular Uptake of SSZ/Ce-Some by BMDMs

To study the internalization in macrophages, Cy5-labeled SSZ/Ce-Some was prepared similarly as in Section 4.1 except that 0.5 wt % Cy5-labeled PEG-P(TMC-DTC) was premixed with 99.5 wt % PEG-P(TMC-DTC)-PAsp. BMDMs were cultured overnight in a 6-well plate (1×10^6/well) and treated with PBS or LPS (100 ng/mL)/IFN-γ (10 ng/mL) for 12 h to acquire M0 macrophages (M0M) or M1 macrophages (M1M). Then, Cy5-labeled SSZ/Ce-Some (Ce: 5 μg/mL, SSZ: 50 μg/mL, Cy5:0.1 μg/mL) was added to incubate at 37 °C (n = 3). At 2, 4, or 12 h, cells were washed twice with PBS, resuspended in 500 μL of PBS, and immediately measured using a flow cytometer.

For the endocytic pathway study, M1M were added respectively with endocytosis inhibitors, nystatin, genistein, amiloride, wortmannin, chlorpromazine and dynasore at 37 °C. After incubation for 1 h, Cy5-labeled SSZ/Ce-Some was added and incubated for 4 h without changing the medium. Cells were collected, washed twice with PBS, resuspended in 500 μL of PBS, and immediately measured using a flow cytometer. M1M directly treated with PBS, Cy5-labeled SSZ/Ce-Some or nonlabeled SSZ/Ce-Some, as well as M1M directly treated with Cy5-labeled SSZ/Ce-Some at 4 °C were studied for comparison. Using the same schedule, the endocytic pathway of Cy5-labeled SSZ/Ce-Some by M0M was studied.

2.5. Anti-Inflammatory Effects and Immune Regulation In Vitro

BMDMs cultured in 12-well plates (1×10^6/well) were stimulated with LPS (100 ng/mL) and IFN-γ (10 ng/mL) for 1 h. SSZ/Ce-Some, Ce-Some, SSZ-Some (Ce: 5 μg/mL, SSZ: 50 μg/mL) and PBS were added and incubated at 37 °C for 24 h (n = 3). Unstimulated cells served as negative control. Culture media were collected to measure the concentrations of IL-6, TNF-α, and IL-10 using ELISA kits. Cells were detached and labeled with anti-CD11b, anti-F4/80, and anti-CD206 antibodies. Flow cytometry was performed to analyze the M1/M2 ratio (M1M: $CD206^-$; M2M: $CD206^+$).

BMDCs seeded in 12-well plates (1×10^6/well) were stimulated with LPS (100 ng/mL) for 1 h. SSZ/Ce-Some, Ce-Some, SSZ-Some, and PBS were added and incubated at 37 °C for 11 h (n = 3). Culture media were collected for quantification of cytokines using ELISA kits and cells were labeled with anti-CD11c and anti-CD86 antibodies for flow cytometry measurement of activated $CD86^+$DCs.

2.6. Deposition in Inflamed Colonic and Biodistribution of SSZ/Ce-Some in UC Mice

All animal experiments were performed in accordance with the Guidelines for Care and Use of Laboratory Animals of Soochow University (P.R. China) and approved by the Animal Ethics Committee of Soochow University (approval numbers: 202412A1005, 202508A0096).

The acute ulcerative colitis (UC) models were built in C57BL/6 mice by giving 3% DSS solution as drinking water for five successive days. Mice were injected intraperitoneally with a single Cy5-labeled SSZ/Ce-Some (200 μL, 0.2 μg Cy5/mouse). At 4, 10, and 24 h postinjection, mice were sacrificed. Colonic tissues, main organs, and mesenteric lymph nodes (MLN) were isolated (n = 3). After PBS washing, ex vivo imaging was performed using IVIS imaging system and fluorescence intensity were semiquantified. Colonic tissues were prepared to obtain single cell suspensions, and stained with anti-CD45, anti-CD11b, anti-F4/80, anti-CD206, anti-CD86, or anti-CD11c to determine the uptake of SSZ/Ce-Some and activation of immune cells.

In a separate group, at 24 h postinjection, colon and MLN were sectioned and stained with anti-F4/80 and DAPI antibodies to reveal the localization of SSZ/Ce-Some.

2.7. SSZ/Ce-Some Treatment of UC Model

UC models were given 3% DSS water (starting from day 0) for 5 days, and on days 5, 7, 9, and 11, SSZ-Some (10 mg/kg), Ce-Some (0.5 mg/kg), Ce-Some (2 mg/kg), SSZ/Ce-Some (Ce/SSZ: 0.5/10 mg/kg), or SSZ/Ce-Some (Ce/SSZ: 2/10 mg/kg) were injected intraperitoneally (n = 4). PBS-treated mice and healthy mice served as controls. Body weight was monitored daily, and the disease activity index (DAI) was calculated based on weight loss percentage, stool consistency, and presence of rectal bleeding, as reported in the literature.[19] Mice were sacrificed on day 12, and colon was photographed and measured. Colon tissue (100 mg) was homogenized for 10 min, and added to 500 μL lysis buffer (containing 1% Triton X-100). After centrifugation (1000 rpm, 5 min), supernatant was used for cytokine quantification (TNF-α, IL-6, IL-1β, IL-10) using ELISA. The remaining tissue was fixed in 4% paraformaldehyde, paraffin-embedded, sectioned, and stained with hematoxylin−eosin (H&E), myeloperoxidase (MPO), and tight junction protein antibodies (zonula occludens-1 (ZO-1) and occludin) for pathological analysis.

2.8. SSZ/Ce-Some Treatment of TNBS-Induced CD Models

Chronic Crohn's Disease (CD) models were established according to a reported method but with modifications.[20] Briefly, C57BL/6 mice were presensitized by topical application of 1% TNBS in ethanol/PBS solution to the shaved dorsal skin to prime hapten-specific immune responses and develop chronic intestinal inflammation. One week later, anesthetized mice received weekly, via a 8 cm catheter in the rectum, intrarectal administration of 100 μL TNBS for 6 weeks at increasing concentrations of 0.75%, 1.5%, 2.5%, 2.5%, 2.5%, and 2.5%, respectively (n = 5). After each injection, mice were inverted for 1−3 min to prevent fluid leakage.

During the induction process, at 24 and 72 h after the third, fourth, fifth, and sixth intrarectal TNBS administration, mice received oral gavage of 400 μL SSZ/Ce-Some@gel (Ce/SSZ equivalent dose: 2/10 mg/kg) (n = 5). CD mice receiving only PBS and healthy mice without treatment were used as controls. Body weight and DAI were recorded daily to assess disease severity. On day 50, mice were euthanized and main organs were collected, and colons were photographed and measured. About 1 cm distal colonic segments were excised at 1 cm proximal to the anal verge, and processed for histopathological evaluation, including H&E staining, MPO immunohistochemistry, and immunofluorescence staining for ZO-1 and occludin. Inflamed colonic tissues (100 mg) were homogenized, and subject to lysis. After centrifugation, supernatant was used for cytokine quantification (TNF-α, IL-6, IL-10) by ELISA. Colon, MLNs and spleen were prepared for single cell suspension, and macrophages (anti-CD11b, anti-F4/80, anti-CD206), DCs (anti-CD11c, anti-CD80, anti-MHCII), B cells (anti-CD69, anti-B220), Tregs (anti-CD3, anti-CD4, anti-CD25, anti-Foxp3) and Th1 (anti-CD3, anti-CD4, anti-CXCR3) were labeled with corresponding antibodies.

2.9. Statistical Analysis

Data are presented as mean ± standard deviation. Data were processed and analyzed using GraphPad Prism 9.0. Mouse survival was analyzed using the log-rank (Kaplan−Meier) test. Group differences were assessed by one-way ANOVA followed by Tukey's multiple comparison test or Student's t test. Statistical significance was set as $^*p < 0.05$, $^{**}p < 0.01$, $^{***}p < 0.001$, and $^{****}p < 0.0001$ as highly significant differences.

3. RESULTS AND DISCUSSION

3.1. Preparation and Physicochemical Characterization of SSZ/Ce-Some

SSZ/Ce-Some was constructed by coassembling PEG-P(TMC-DTC)-PAsp with cerium ions and SSZ in HEPES buffer (pH 6.8, 5 mM), during which multivalent coordination between cerium ions with carboxylate groups of poly(aspartic acid) segment and SSZ occurred concurrently with disulfide cross-linking within polymersomal membrane. This one-pot assembly yielded stable vesicular nanostructures capable of simultaneously accommodating redox-active cerium ions and a clinically approved small-molecule drug. Control formulations containing only SSZ (SSZ-Some) or cerium ions (Ce-Some)

https://doi.org/10.1021/acs.biomac.6c00702
Biomacromolecules 2026, 27, 4734−4746

Table 1. Characteristics of SSZ/Ce-Some (n = 3)

	Ce loading		SSZ loading				
sample	DLC[a] wt %	DLE[a] %	DLC[b] wt %	DLE[b] %	size[c] (nm)	PDI[c]	zeta potential[d](mV)
SSZ/Ce-Some1/5	1.5	84.6	7.2	86.4	25.0	0.1	−5.5
SSZ/Ce-Some1/10	1.5	83.8	15.8	87.2	25.0	0.1	
SSZ/Ce-Some1/20	1.5	83.8	23.1	85.6	25.0	0.1	
Ce-Some	1.5	85.7			33.0	0.1	−0.1
SSZ-Some			8.3	86.4	24.0	0.1	

[a]Determined by ICP-OES. [b]Measured by UV. [c]Determined by DLS at 25 °C in HEPES (5 mM, pH 7.4). [d]Determined by Zetasizer Nano-ZS at 25 °C in in HEPES (5 mM, pH 7.4).

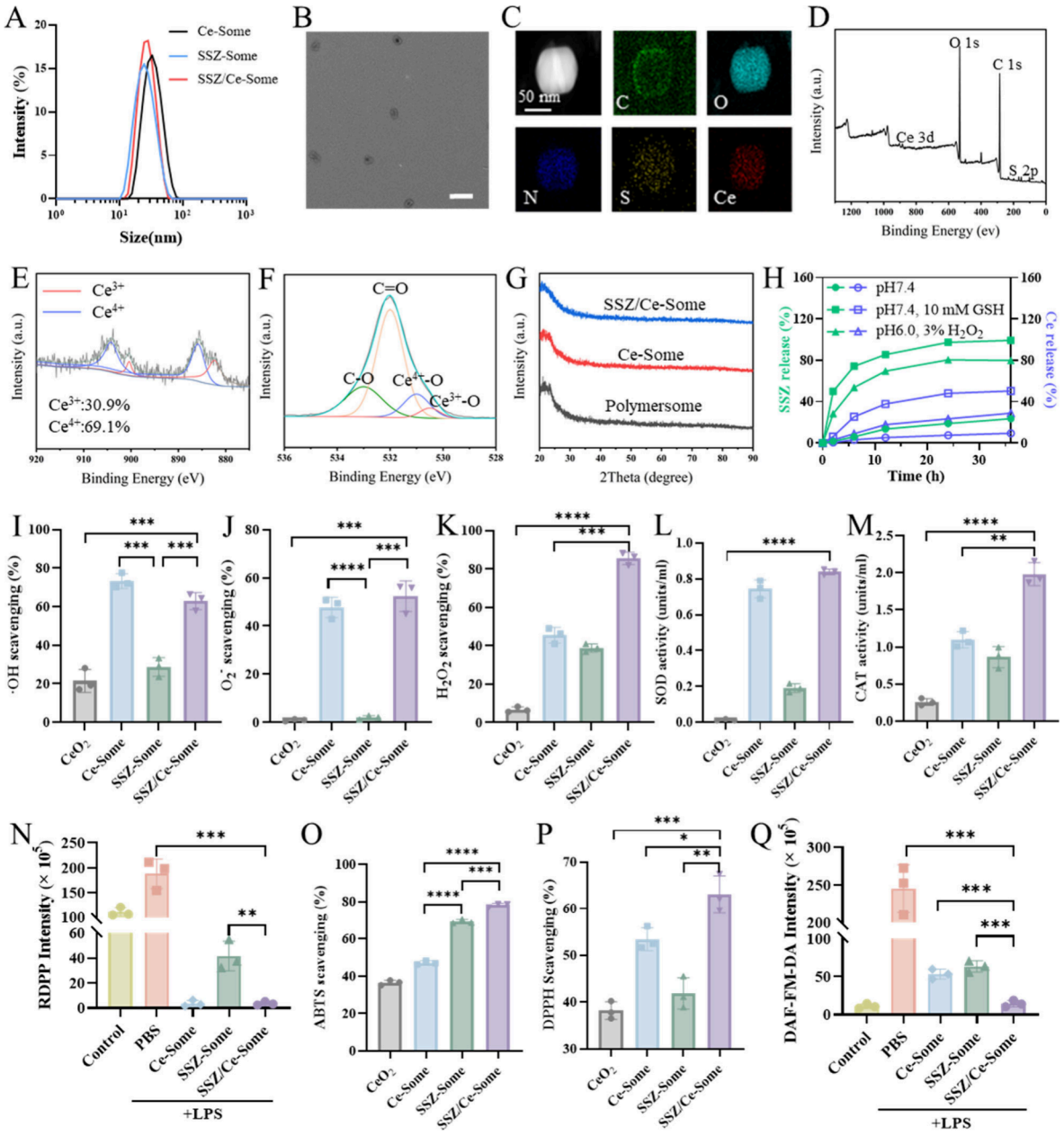

Figure 1. Characterization of SSZ/Ce-Some. Size distribution determined using (A) DLS and (B) TEM (scale bar: 50 nm). (C) STEM-EDS mapping of SSZ/Ce-Some. (D) XPS patterns of SSZ/Ce-Some and high-resolution spectra of (E) Ce 3d and (F) O 1s. (G) XRD spectra of SSZ/Ce-Some, Ce-Some and empty polymersomes. (H) Drug release profiles of SSZ and Ce ions under various conditions (n = 3). Scavenge efficacy of (I) $^{\bullet}OH$, (J) $O_2^{-\bullet}$ and (K) H_2O_2, as well as (L) SOD-like and (M) CAT-like catalytic activities of SSZ/Ce-Some. (N) Intracellular hypoxia levels of BMDM treated with SSZ/Ce-Some. Scavenging of (O) ABTS and (P) DPPH. (Q) Intracellular NO levels of BMDM treated with SSZ/Ce-Some.

were prepared using identical protocol. Previous investigations have confirmed the vesicular structure of the small nanoparticles formed from PEG-P(TMC-DTC)-PAsp triblock copolymers with PAsp repeating units of 5 to 10 and 15, with Cryo-TEM

https://doi.org/10.1021/acs.biomac.6c00702
Biomacromolecules 2026, 27, 4734−4746

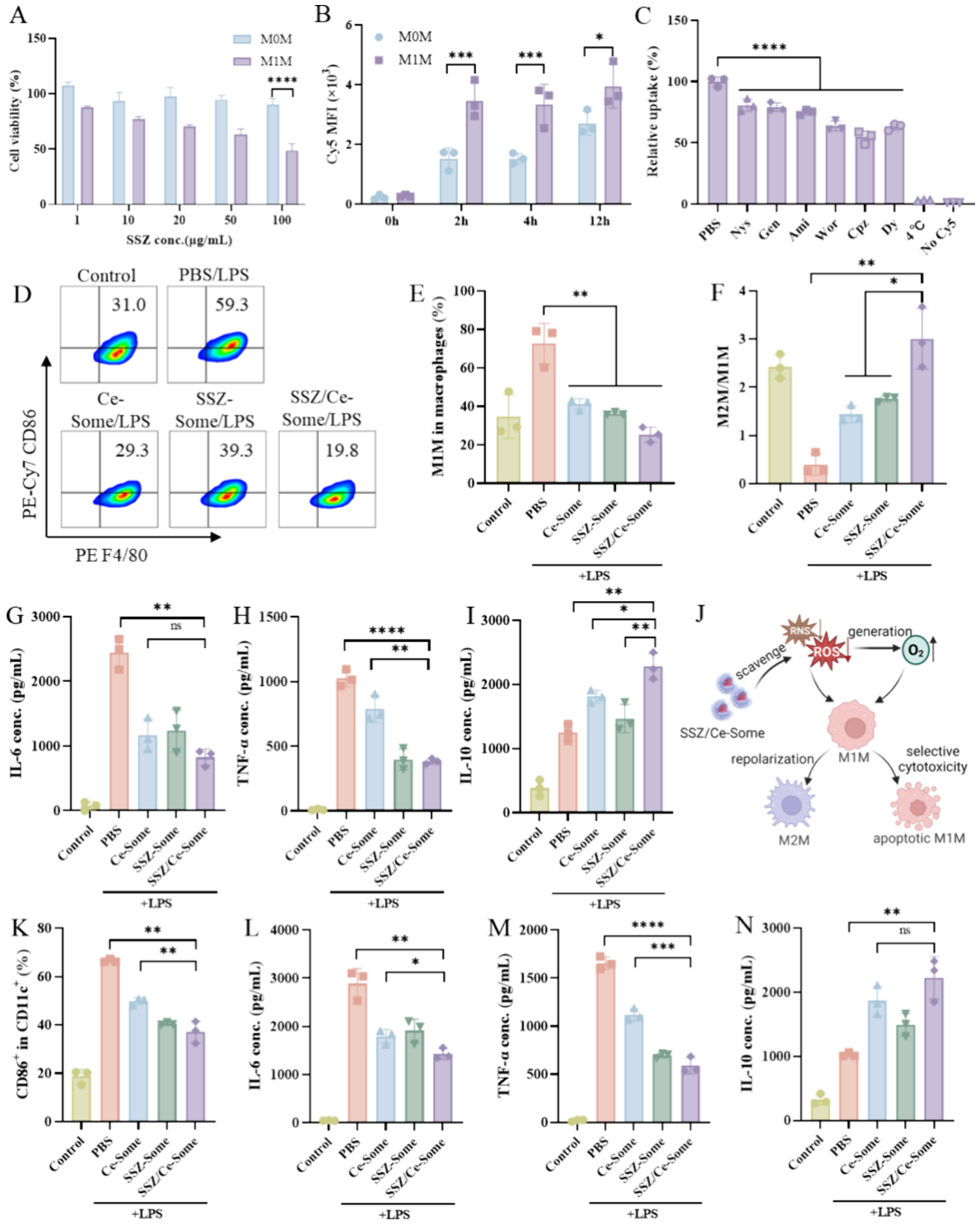

Figure 2. In vitro redox immune modulation in macrophages and DCs (n = 3). (A) Viability and (B) internalization of M0M and M1M treated with SSZ/Ce-Some. (C) Endocytotic pathway study of SSZ/Ce-Some in M1M (n = 3). (D) Flow cytometric plots and (E) proportions of M1M, (F) M2M/M1M ratio, and levels of (G) IL-6, (H) TNF-α, and (I) IL-10 secreted by BMDMs at 24 h incubation with SSZ/Ce-Some. (J) Illustration of SSZ/Ce-Some's dual-action on M1M. (K) Proportions of mDCs and secretion of (L) IL-6, (M) TNFα, and (N) IL-10 of DCs at 24 h incubation with SSZ/Ce-Some. Ce-Some, SSZ-Some, and PBS were used as controls. Ce conc.: 5 μg/mL, SSZ conc.: 50 μg/mL.

images showing diameters decreasing from 29 nm to 21 and 16 nm for and static light scattering measurements showing R_g/R_h values ranging from 0.92 to 0.99, in accordance with a vesicular structure.[21]

By varying the Ce/SSZ mass ratio (1/5, 1/10 to 1/20) at a fixed cerium content and a predefined Ce^{3+}/Ce^{4+} ratio (3/7), SSZ/Ce-Some showed high and reproducible loading efficacies for both SSZ and cerium (~85%), corresponding to SSZ loading content of up to 23.1 wt % and cerium loading content of 1.5 wt % (Table 1). DLS measurements showed that SSZ/Ce-Some had an average size of 24 nm (PDI of 0.1) and a slightly negative surface potential (−5.5 mV). TEM images confirmed the

https://doi.org/10.1021/acs.biomac.6c00702
Biomacromolecules 2026, 27, 4734−4746

formation of small spherical vesicles (Figure 1A,B, Table 1). STEM-EDS elemental mapping results revealed homogeneous distribution of C, O, S, and N throughout the nanostructure (Figure 1C). SSZ-Some and Ce-Some had comparable drug loading contents, particle sizes, and zeta potentials as SSZ/Ce-Some (Table 1), and used as control groups in subsequent experiments. To illustrate how Ce ions interact with polymer, FT-IR and UV−vis measurements of Ce-Some were performed. FT-IR spectra showed that the characteristic peaks of Ce-Some at 1277 cm^{-1} (νC−OH) and 920 cm^{-1} (νO−H) exhibited reduced intensities compared to empty vesicles (Figure S1A), and the UV spectrum of Ce-Some displayed a new peak in the range of 250−290 nm (Figure S1B), both ascribable to the coordination of the carboxyl groups of copolymers with Ce ions. The stable coordination between cerium and carboxyl groups, which has been reported in multiple studies,[22] rather than mere salt loading, ensures the stability of the cerium loading within polymersomes, preventing early leakage. Moreover, XPS deconvolution of Ce 3d peaks confirmed the coexistence of Ce^{3+}/Ce^{4+} species at the designed ratio (ca. 3:7), and O 1s spectra feature supported coordination interactions (Figure 1D−F). Notably, the absence of characteristic crystalline diffraction peaks in XRD patterns for SSZ/Ce-Some and Ce-Some (Figure 1G) verifies the noncrystalline, atomically dispersed nature of cerium species within SSZ/Ce-Some.

SSZ/Ce-Some remained colloidally stable with minimum cerium leakage after prolonged storage at 4 °C for 1 month or incubation in media containing 10% FBS (Figure S2). Interestingly, SSZ was released quickly under acidic/oxidative conditions (pH 6.0, 3% H_2O_2) and reductive conditions (pH 7.4, 10 mM GSH), mimicking an inflamed intestinal microenvironment and intracellular cytosolic conditions, respectively, contrasting to the significantly more stable retention of cerium ions (Figure 1H). Such a stimulus-responsive profile is advantageous for localized drug action while maintaining systemic stability.

3.2. Integrated ROS and RNS Scavenging and Antioxidant Capacity of SSZ/Ce-Some

Oxidative and nitrosative stress constitute intertwined pathological drivers in inflamed colons. We therefore evaluated the capacity to neutralize representative ROS and RNS. SSZ/Ce-Some exhibited efficient scavenge ability of $^{\bullet}OH$ and $O_2^{\bullet-}$ comparable to that of Ce-Some but significantly superior to SSZ-Some and the cerium oxide nanoparticle (CeNPs); while for H_2O_2 decomposition, SSZ/Ce-Some outperformed both monotherapies (Figure 1I−K). These results underscore the catalytic advantage conferred by atomically dispersed cerium centers. Consistent with its efficient elimination of $O_2^{\bullet-}$ and H_2O_2, SSZ/Ce-Some displayed robust SOD- and CAT-like catalytic activities (Figure 1L,M). In particular, it exhibited a synergistically enhanced H_2O_2 decomposition and CAT activity. Furthermore, SSZ/Ce-Some as a nanozyme exhibited superior stability and durability compared to natural enzymes. The activity of natural enzymes decreased significantly both at 4 and 37 °C, while SSZ/Ce-Some maintained high CAT-like and SOD-like activity (above 90% of original value) after a 7 day storage (Figure S3A,B). SSZ/Ce-Some also kept high CAT- and SOD-like activities in serum solutions (Figure S3C,D). Correspondingly, pronounced oxygen generation was observed within the M1 phenotype of BMDMs (M1M), a representative in vitro inflammatory model (Figure 1N). This feature is particularly relevant to inflamed colonic tissues, where hypoxia exacerbates epithelial injury and immune activation.[23,24] SSZ/Ce-Some also exhibited the highest clearance efficiencies for stable radicals $ABTS^{\bullet+}$ and $DPPH^{\bullet}$ (Figure 1O,P), suggesting enhanced broad-spectrum radical-scavenging capacity.

Furthermore, the broad free-radical-quenching capability associated with RNS regulation was assessed by examining the intracellular NO levels in M1M using DAF-FM DA staining. Inflammatory stimulation induced strong NO-associated fluorescence, indicating excessive intracellular NO accumulation. Remarkably, SSZ/Ce-Some most effectively suppressed intracellular NO signals, substantially exceeding both Ce-Some and SSZ-Some (Figure 1Q, Figure S4), confirming that its radical-scavenging capability can be translated into biologically relevant regulation of RNS and nitrosative stress in inflammatory cells. It is noted that SSZ-Some exhibited weaker scavenging activity against $^{\bullet}OH$, $O_2^{\bullet-}$ and $DPPH^{\bullet}$, comparable activity against H_2O_2, and much higher activity against $ABTS^{\bullet+}$ as compared to Ce-Some. Remarkably, coencapsulation of SSZ and Ce ions within a single polymersome, SSZ/Ce-Some, achieved complementary scavenging of multiple free radicals, thus broadening the scavenging spectrum of ROS and RNS. This finding is fully demonstrated by the superior comprehensive effects of SSZ/Ce-Some in intracellular oxygen generation and NO scavenging assays.

The concurrent clearance of both $O_2^{\bullet-}$ and NO is of particular importance in the context of IBD, because these two species can rapidly react to generate peroxynitrite ($ONOO^-$), which is one of the most destructive RNS in inflamed intestinal tissues, and is known to induce protein nitration, lipid peroxidation, and mitochondrial dysfunction, thereby disrupting epithelial barrier integrity and delaying mucosal repair.[25−27] Collectively, these results indicate that SSZ/Ce-Some broadens redox coverage beyond conventional ROS-centered antioxidant strategies and may provide a more comprehensive means of controlling oxidative−nitrosative stress in IBD.

3.3. Regulation of Pro-Inflammatory Macrophages and Dendritic Cells In Vitro

Macrophages exposed to inflammatory cues are major sources and amplifiers of RONS in IBD. Using LPS-stimulated BMDMs as an in vitro model, we evaluated the immunomodulatory effects of SSZ/Ce-Some under inflammatory conditions. SSZ/Ce-Some induced pronounced, dose-dependent cytotoxicity toward M1 macrophages (M1M) that predominate at inflamed sites, reducing cell viability to 48% at SSZ of 100 μg/mL (Ce: 10 μg/mL; Figure 2A), while minimal effect was observed on naïve macrophages (M0M) or intestinal epithelial cells (Figure 2A, Figure S5), demonstrating a favorable safety profile. Cellular uptake studies revealed preferential internalization of Cy5-labeled SSZ/Ce-Some by M1M relative to M0M (Figure 2B), consistent with their heightened phagocytic activity[28] and high cytotoxicity to M1M. Endocytosis inhibition experiments revealed that SSZ/Ce-Some uptake involved multiple pathways, including caveolae-mediated, clathrin-mediated, and macropinocytotic processes (Figure 2C, Figure S6), and the internalization was markedly suppressed upon dynamin inhibition and nearly eliminated at 4 °C, confirming an active, highly energy-dependent internalization mechanism.

Beyond direct cytotoxicity, at subcytotoxic concentrations, SSZ/Ce-Some exhibited a great capacity of repolarizing M1M to M2-like reparative phenotype (M2M), showing a reduced proportion from 59.3% to 19.8% and the highest M2M/M1M ratio (1.5−2-fold higher than monotherapies) (Figure 2D−F).

https://doi.org/10.1021/acs.biomac.6c00702
Biomacromolecules 2026, 27, 4734−4746

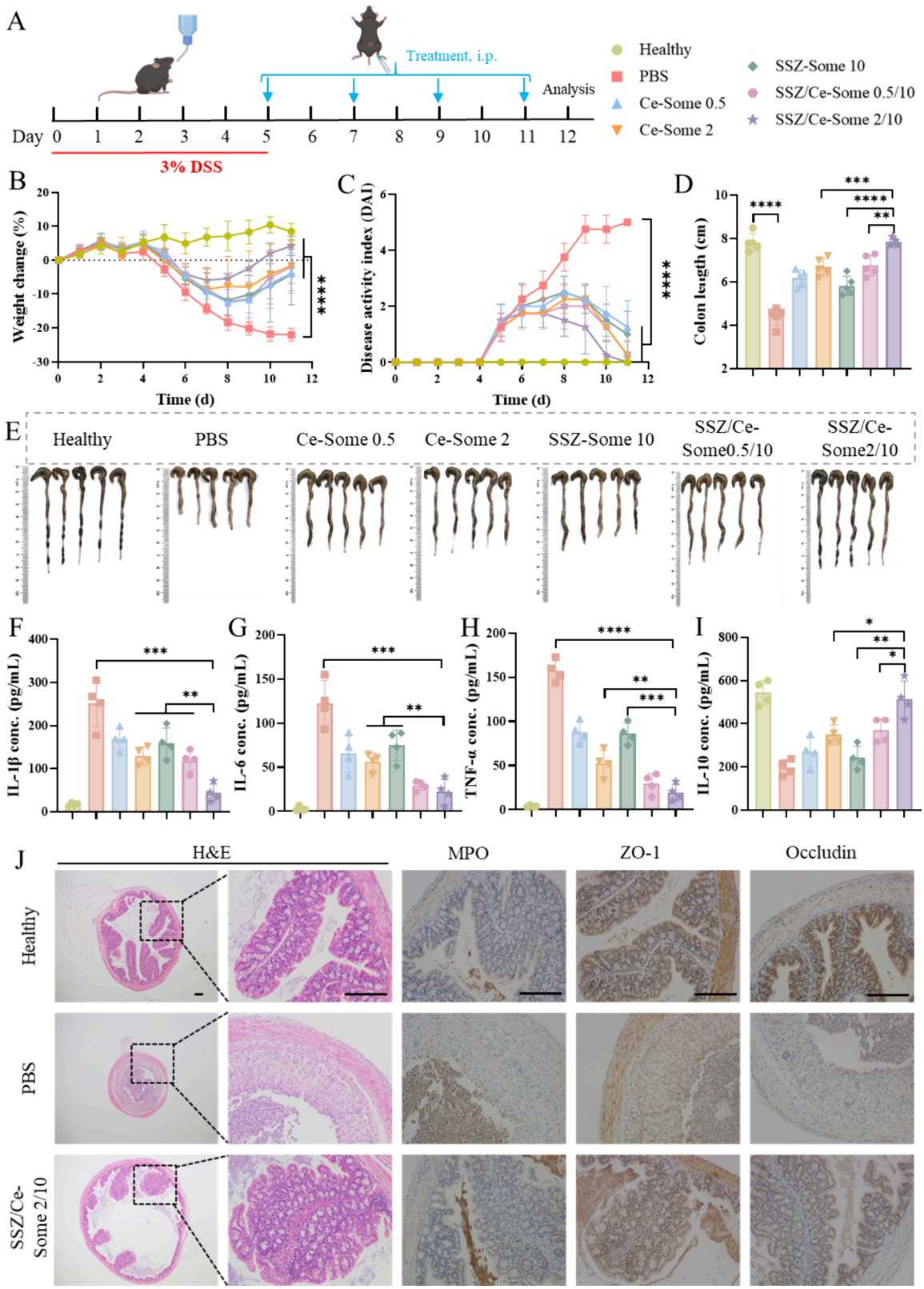

Figure 3. Therapeutic efficacy of SSZ/Ce-Some in UC models (n = 5). (A) Treatment scheme (Ce doses: 0.5 or 2 mg/kg; SSZ dose: 10 mg/kg). Changes in (B) body weight and (C) disease activity index during the treatment. (D) Length (data are shown as mean ± SEM) and (E) photographs of colons. Contents of (F) IL-1β, (G) IL-6, (H) TNFα and (I) IL-10 in colon tissues on day 12. (J) Pathological images of inflamed colon slices stained with H&E, MPO, ZO-1 and occludin (scale bar: 200 μm).

Concurrently, this phenotypic shift was accompanied by marked suppression of pro-inflammatory cytokines (IL-6, TNF-α) and elevation of anti-inflammatory reparative cytokine IL-10 (Figure 2G–I), confirming relieved inflammation, which consequently reduce RONS generation and epithelial barrier damage.[29,30] These results illustrate that SSZ/Ce-Some elicits dual-action on

https://doi.org/10.1021/acs.biomac.6c00702
Biomacromolecules 2026, 27, 4734–4746

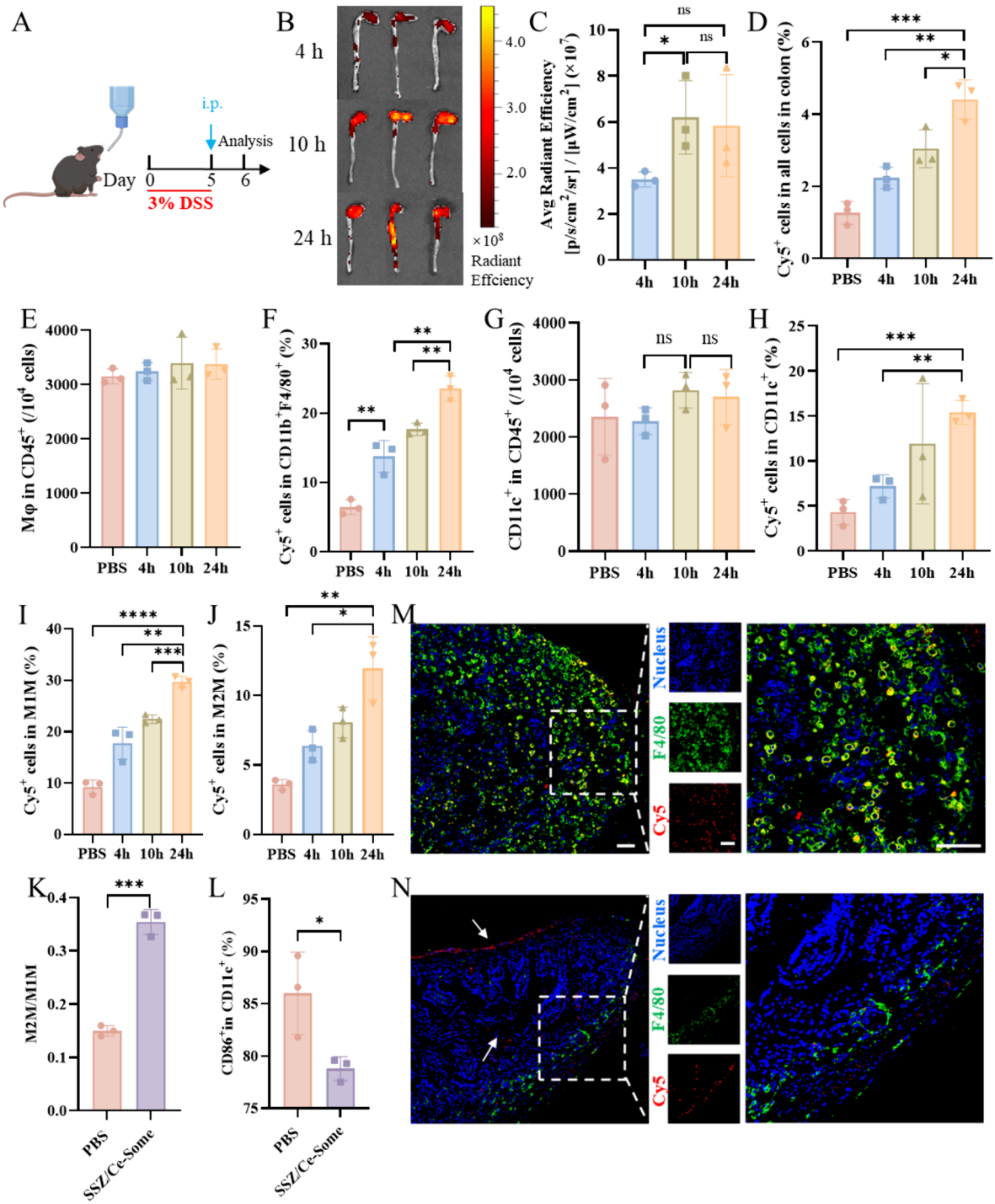

Figure 4. Colonic deposition of SSZ/Ce-Some and M1M repolarization upon i.p. injection ($n = 3$). (A) Experimental schedule in IBD mouse models. (B) Ex vivo images and (C) semiquantification of colon average fluorescence with time ($n = 3$). (D) Percentage of $Cy5^+$ cells in total colonic cells. (E) Counts of macrophages ($CD11b^+F4/80^+$) in $CD45^+$ cells and (F) their $Cy5^+$ cell proportions. (G) Counts of $CD11c^+$ cells in $CD45^+$ cells and (H) their $Cy5^+$ cell proportions. $Cy5^+$ cell contents in (I) M1M and (J) M2M. (K) M2M/M1M ratio and (L) contents of mature DCs in colons at 24 h postinjection. Immunostaining CLSM images of (M) MLN and (N) colon tissues of IBD mice received i.p. injection of Cy5-labeled SSZ/Ce-Some (FITC-labeled $F4/80^+$ antibody stained macrophages, DAPI stained nuclei, scale bars: 50 μm).

M1M: direct selective cytotoxicity and modulation into pro-reparation M2M via potent antioxidant activity and hypoxia mitigation (Figure 2J).

In parallel, SSZ/Ce-Some significantly attenuated dendritic cell (DC) maturation, reducing the proportion of $CD86^+$DCs (mDC) and associated inflammatory cytokine IL-6 and TNF-α secretion (Figure 2K–N). mDCs, as key antigen-presenting cells, play important roles in inflammation and showed great activation in LPS-stimulated model group.[31] These results indicate that SSZ/Ce-Some modulates the inflammatory immune microenvironment and disrupts key cellular circuits that perpetuate inflammatory signaling in IBD through coordinated redox regulation and immune cell reprogramming rather than through a single cytotoxic mechanism.

https://doi.org/10.1021/acs.biomac.6c00702
Biomacromolecules 2026, 27, 4734−4746

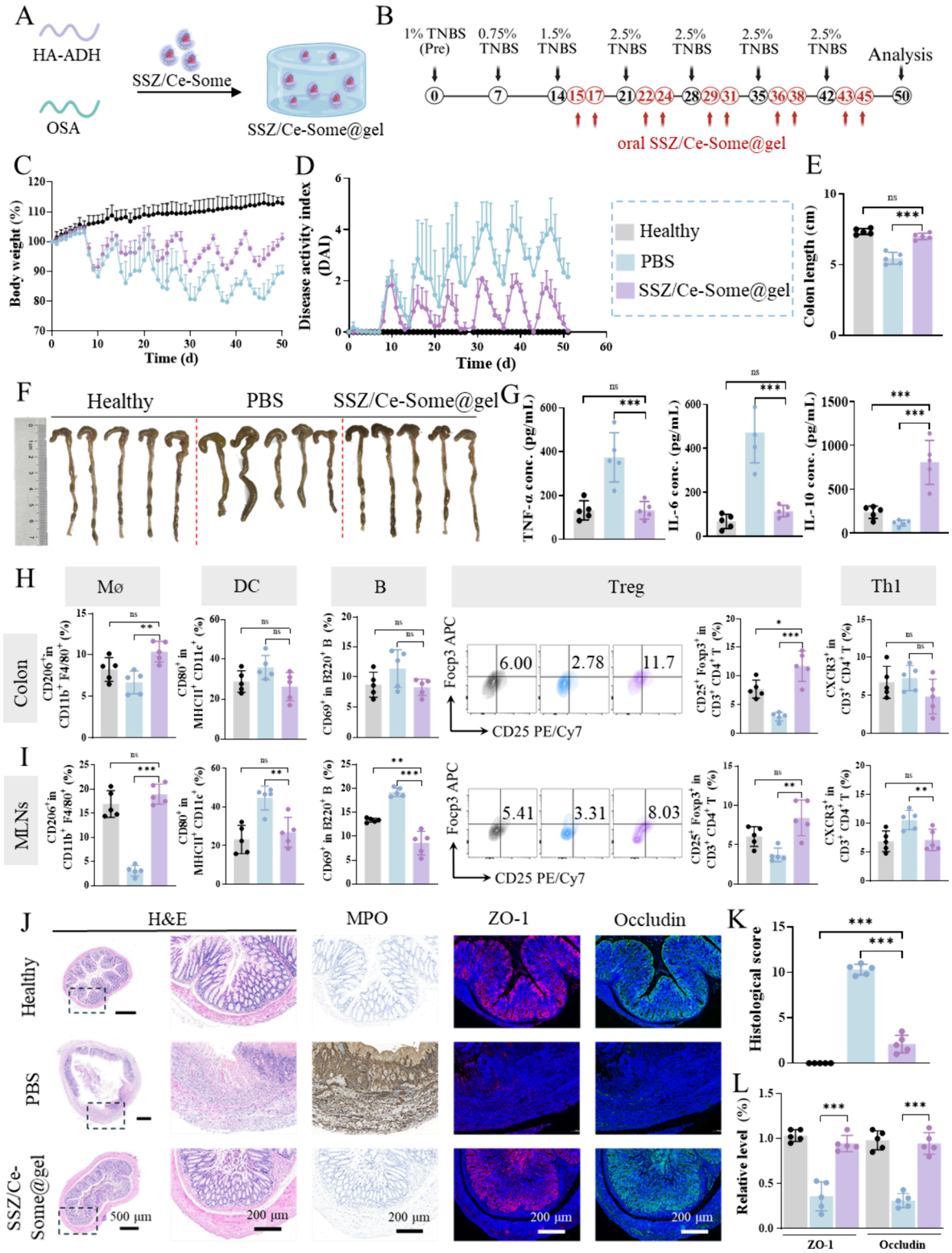

Figure 5. Therapeutic efficacy of SSZ/Ce-Some in TNBS-induced chronic CD model via oral administration with a mucoadhesive gel (n = 5). (A) Schematic formation of SSZ/Ce-Some embedded hydrogel SSZ/Ce-Some@gel (Ce dose: 2 mg/kg; SSZ dose: 10 mg/kg in each 50 μL hydrogel). (B) CD model established and treatment scheme. Changes in (C) body weight and (D) DAI during the treatment. (E) Length, (F) photographs, and (G) contents of TNFα, IL-6, and IL-10 of the colon on day 50. Proportions of M2M, activated DC, activated B cells, Treg, and Th1 in (H) colon and (I) MLNs. (J) Pathological images of inflamed colon slices stained with H&E, MPO, ZO-1 and occludin (scale bar: 200 μm). (K) Colonic histological scores calculated from H&E sections and (L) fluorescence intensity quantification of ZO-1 and occludin.

https://doi.org/10.1021/acs.biomac.6c00702
Biomacromolecules 2026, 27, 4734−4746

3.4. Therapeutic Activity and Barrier Protection of SSZ/Ce-Some in UC Models

The in vivo therapeutic performance of SSZ/Ce-Some was evaluated in 3% DSS induced acute UC models (Figure 3A). SSZ is commonly administered orally in clinical practice, but its oral bioavailability is relatively low (10−15%), necessitating high doses (3−4 g daily) and thereby increasing the incidence of adverse effects. This study thus explored the in vivo therapeutic efficacy of SSZ/Ce-Some following intraperitoneal (i.p.) administration. PBS mice started diarrhea and lost body weight from day 4, showing a rapidly increased disease activity index (DAI). In contrast, all i.p. administered nanoformulations led to body weight recovery and DAI decline from day 8 (Figure 3B,C). In particular, SSZ/Ce-Some 2/10 group exhibited the least variations in body weight and DAI with the fastest recovery, resumed a healthy status from day 11. Colon shortening, as a key feature of colitis (PBS colons: ∼4.5 cm; healthy colons: ∼7.8 cm), was significantly alleviated by SSZ/Ce-Some in a Ce-content-dependent manner and was basically prevented by SSZ/Ce-Some 2/10 treatment (Figure 3D,E). Analysis of colonic cytokines revealed that substantial decreases in IL-6, IL-1β and TNF-α, alongside recovery of reparative IL-10 levels, also in a Ce content-dependent manner. Again, SSZ/Ce-Some 2/10 group regulated the secreted cytokines to near-physiological levels (Figure 3F−I). These results collectively illustrate that among all test formulations, SSZ/Ce-Some 2/10 exhibited the most pronounced therapeutic benefit, restoring clinical parameters to near-healthy levels.

Colonic injury to epithelial cells and mucosal barrier is a key pathological feature of IBD, and is highly challenging to reverse or prevent. Here, our histopathological examination demonstrated preservation of nearly intact mucosal architecture and crypt morphology, and minimal inflammatory infiltration in SSZ/Ce-Some-treated mice, contrasting severe epithelial damage and unresolved inflammation (MPO) in PBS group (Figure 3J). Monotherapies only partially restored mucosa but could not rescue crypt morphology. Immunofluorescence staining further confirmed restoration of tight junction proteins ZO-1 and occludin, verifying the successful barrier repair. Furthermore, H&E staining images showed no obvious toxicity in the major organs of mice after SSZ/Ce-Some treatment (Figure S7). The suppression of tissue-disruptive peroxynitrite species by SSZ/Ce-Some, via concurrent clearance of superoxide and NO, as well as oxygen-generating capability, may be particularly beneficial for limiting epithelial damage and facilitating barrier restoration.

3.5. Colonic Accumulation and Immune Cell Engagement in UC Models upon i.p. Injection

Deposition of Cy5-labeled SSZ/Ce-Some within inflamed colons of UC models following i.p. injection was then investigated (Figure 4A). The ex vivo imaging illustrated a preferential accumulation at inflammatory sites at 4 h with sustained retention up to 24 h (Figure 4B,C). Such high accumulation and prolonged retention at inflamed colons ensured potent treatment efficacy in Figure 3. Flow cytometry analysis to identify the types of cells internalizing SSZ/Ce-Some confirmed the increasing association of SSZ/Ce-Some with immune cell populations in the colon, particularly macrophages ($CD11b^+F4/80^+$) and $CD11c^+$ cells. SSZ/Ce-Some uptake proportion in total colonic cells increased ca. 3.5-fold from 0 to 24 h (Figure 4D), and their internalization in macrophages and $CD11c^+$ cells increased ca. 4-fold (Figure 4E−H), despite nearly constant total populations. It was reported that $CD11b^+F4/80^+$ cells and $CD11c^+$ cells account for 30−40% and 15−30% in IBD mice, respectively.[32] While accumulation in both M1M and M2M were augmented with time (Figure 4I,J), at 24 h the M2M/M1M ratio resulted in ca. 2.5-fold elevation, revealing the in vivo repolarization capacity of SSZ/Ce-Some (Figure 4K). Concurrently, colonic-activated $CD86^+CD11c^+$ cells were significantly reduced (Figure 4L). It is known that $CD11c^+$ cells include DCs and inflamed monocytes and small-intestine-specific cDC subsets at the mucosal surface or crypt base in inflammatory colons, and these cDCs can be reprogrammed to sustain inflammation by bacterial products and pro-inflammatory cues to favor Th1/Th17 responses.[33]

To study transport pathways of SSZ/Ce-Some following i.p. administration, we examined colons and mesenteric lymph nodes (MLN) that play an important role in the occurrence and progression of IBD.[34] Histological immunofluorescence imaging revealed the abundance of macrophages (green) and their high colocalization with SSZ/Ce-Some (red) in MLN slices at 24 h (Figure 4M). In colon sections, one side displayed many macrophages containing SSZ/Ce-Some, presumably the side proximal to MLN, while on the opposite side many dispersed SSZ/Ce-Some (white arrows) but scarce macrophages were observed (Figure 4N). Dispersed SSZ/Ce-Some were present at both sites and within colons. Accordingly, SSZ/Ce-Some was delivered to colonic lesions possibly through both macrophage-mediated transport and passive trans-serosal migration, enabling rapid enrichment and retention at inflamed sites for synergistic action of suppressing inflammation. It is noted that macrophage-mediated transport strategy has been applied for drug delivery. In most of these studies, however, macrophages were employed either as passive carriers that sequester nanoparticles or as ex vivo-engineered cellular vehicles.[35−37] In this study, unlike ex vivo adoptive transfer, which is limited by complex manufacturing and impaired cell homing, SSZ/Ce-Some employs an in vivo hitchhiking strategy. Anatomically, the peritoneal cavity provides an abundant reservoir of macrophages that naturally migrate to inflamed colonic niches. Following i.p. administration, SSZ/Ce-Some may be taken up by peritoneal macrophages, and these cells subsequently migrate to inflamed tissues via the lymphatic or blood circulation.

3.6. Oral SSZ/Ce-Some@gel Restores Immune Homeostasis in Chronic Crohn's Disease Models

SSZ/Ce-Some therapy was further evaluated in a clinically relevant, refractory chronic TNBS-induced Crohn's Disease (CD) model. CD as an autoimmune disease is characterized by multifactorial pathogenesis involving genetic susceptibility, immune dysregulation, and microbiota imbalance.[38] TNBS induces a Th1-dominated immune response and specifically causes transmural inflammation, successfully recapitulating the core pathological features of CD patients.[39] Current therapies, including immunosuppressants and biologics, induce variable therapeutic response, but recurrence is almost inevitable.[40] SSZ/Ce-Some was incorporated into a mucoadhesive oral hydrogel (SSZ/Ce-Some@gel) for prolonged retention in inflamed colons (Figure 5A). The hydrogel was based on rapid gelation of functionalized hyaluronic acid and alginate through dynamic Schiff-base formation, and demonstrated shear-thinning, acid-resistant and colonic targeting properties (Figure S8).

Chronic CD models were established with stepwise-increased TNBS induction once a week for successive 7 weeks according to a reported protocol[20] with modifications (Figure 5B). After

https://doi.org/10.1021/acs.biomac.6c00702
Biomacromolecules 2026, 27, 4734−4746

each intrarectal TNBS induction, body weight of PBS mice dropped about 15% within 3 days but regained to 80−85% of initial value in 4 days. By day 50, body weight reached 90% of initial value, and DAI scores fluctuated accordingly (Figure 5C,D). These fluctuations effectively recapitulate the chronic and relapsing disease course of CD patients, characterized by alternating active and remission phases in clinical settings. Remarkably, oral administrations of SSZ/Ce-Some@gel achieved amazing therapeutic outcomes and kept the fluctuations much closer to healthy ranges: body weight came back to 100% and DAI was reduced to zero, resuming the healthy state (Figure 5C,D). Colonic length and status largely maintained healthy state, contrasting with the progressive deterioration in PBS group (Figure 5E,F). Colonic local cytokine levels demonstrated that TNF-α and IL-6 were decreased by 3∼4-fold, while IL-10 was increased over 8-fold compared to PBS group, reflecting the extraordinary anti-inflammation and reparative ability (Figure 5G).

Immune profiling confirmed an extensive remodeling of both local and systemic immune landscape. SSZ/Ce-Some@gel treatment demonstrated that proinflammatory environment was favorably regulated, showing significant increase in M2M and suppression of activated DCs and B cells (Figure 5H). Strikingly, Treg ($CD25^+Foxp3^+CD4^+$) proportion was expanded 3.9-fold as compared to PBS group. Treg is considered the most important cells in regulating the tolerant immune environment and maintaining colon homeostasis.[41] Moreover, in MLN and spleen, SSZ/Ce-Some@gel treatment also displayed the highest increment in M2M and Treg and the most suppressed levels of activated DCs and B cells (Figure 5I, Figure S9). Th1 cells secrete IFN-γ and GM-CSF to clear intracellular pathogens via activation/recruitment of monocytes, macrophages and DCs.[42] Interestingly, our treatment significantly reduced systemic Th1 contents to a healthy level. These data further underscore the systemic impact of localized oral therapy, favoring a durable IBD control. Such immune reprogramming may benefit from the remodeling of inflammatory redox microenvironment, as excessive RONS are known to sustain pro-inflammatory activation of myeloid cells.

Histological analyses confirmed the inflammation resolution and nearly complete recovery of colonic tissue architecture and function, with tight junction protein expression and histological score resembling the healthy group (Figure 5J−L). Furthermore, blood biochemistry and hematology analysis showed that all parameters in the SSZ/Ce-Some@gel group had no statistically significant differences compared with the healthy control (Figure S10). These data pinpoint that the oral SSZ/Ce-Some@gel regulated the local and systemic immune landscape, re-established immune tolerance and tissue integrity in chronic intestinal inflammation, leading to long-term successful outcomes in CD models. This extraordinary therapeutic efficacy further suggests that regulation of nitrosative stress may be particularly relevant in persistent intestinal inflammation, where sustained NO overproduction and oxidative−nitrosative imbalance contribute to ongoing tissue injury and impaired mucosal restitution.

4. CONCLUSION

We have developed SSZ/Ce-Some as a redox-regulating and mucosa-protective nanotherapeutic by integrating sulfasalazine with cerium ion-based polymersomes for the treatment of inflammatory colitis. SSZ/Ce-Some not only extended antioxidant intervention from conventional ROS scavenging to coordinated ROS/RNS detoxification, but also coupled this redox-regulating capacity with inflammatory immune-cell suppression and colonic barrier protection. As a result, SSZ/Ce-Some displayed potent therapeutic efficacy in both acute and chronic colitis models. After intraperitoneal administration, SSZ/Ce-Some preferentially accumulated in inflamed colons with prolonged retention, markedly alleviated inflammation, and rapidly controlled acute ulcerative colitis. In chronic Crohn's disease, oral administration of SSZ/Ce-Some in a mucoadhesive hydrogel enabled sustained topical therapy, reduced disease activity, and promoted immune re-education toward a tolerance-associated direction. These findings highlight that rationally integrating clinically used drugs with redox-active nanomedicines may provide an effective strategy to overcome persistent oxidative−nitrosative injury and barrier dysfunction in refractory IBD.

■ ASSOCIATED CONTENT

Supporting Information

The Supporting Information is available free of charge at https://pubs.acs.org/doi/10.1021/acs.biomac.6c00702.

Materials and characterizations; In vitro drug release and durability of enzymatic activity of SSZ/Ce-Some; Synthesis of modified hyaluronic acid; Hydrogel formation and rheological property; Stability study; FT-IR and UV−vis spectra; Intracellular NO clearance capacity; Cytotoxicity and endocytosis of SSZ/Ce-Some; H&E-stained images of major organs; Blood routine parameters of mice (PDF)

■ AUTHOR INFORMATION

Corresponding Authors

Zhiyuan Zhong − *Biomedical Polymers Laboratory, College of Chemistry, Chemical Engineering and Materials Science and College of Pharmaceutical Sciences, Soochow University, Suzhou 215123, P. R. China;* orcid.org/0000-0003-4175-4741; Phone: +86-512-65880098; Email: zyzhong@suda.edu.cn

Fenghua Meng − *Biomedical Polymers Laboratory, College of Chemistry, Chemical Engineering and Materials Science, Soochow University, Suzhou 215123, P. R. China;* orcid.org/0000-0002-8608-7738; Phone: +86-512-65882060; Email: fhmeng@suda.edu.cn

Authors

Miao Sun − *Biomedical Polymers Laboratory, College of Chemistry, Chemical Engineering and Materials Science, Soochow University, Suzhou 215123, P. R. China*

Runkai Lv − *Biomedical Polymers Laboratory, College of Chemistry, Chemical Engineering and Materials Science, Soochow University, Suzhou 215123, P. R. China*

Yongjie Sha − *Biomedical Polymers Laboratory, College of Chemistry, Chemical Engineering and Materials Science, Soochow University, Suzhou 215123, P. R. China*

Luying Zhu − *Biomedical Polymers Laboratory, College of Chemistry, Chemical Engineering and Materials Science, Soochow University, Suzhou 215123, P. R. China*

Jun Cao − *Biomedical Polymers Laboratory, College of Chemistry, Chemical Engineering and Materials Science, Soochow University, Suzhou 215123, P. R. China*

Complete contact information is available at:

https://doi.org/10.1021/acs.biomac.6c00702
Biomacromolecules 2026, 27, 4734−4746

https://pubs.acs.org/10.1021/acs.biomac.6c00702

Author Contributions

[#]These authors contributed equally to this work (M.S. and R.L.).

Notes

The authors declare no competing financial interest.

■ ACKNOWLEDGMENTS

This work is supported by research grants from the National Key Research and Development Program of China (2024YFA1210303, 2022YFA1206001) and the National Natural Science Foundation of China (NSFC 52473142, 52033006). The authors thank Biorender.com for assisting with the illustrations (https://BioRender.com/s01f741).

■ REFERENCES

(1) Ng, S. C.; Shi, H. Y.; Hamidi, N.; Underwood, F. E.; Tang, W.; Benchimol, E. I.; Panaccione, R.; Ghosh, S.; Wu, J. C. Y.; Chan, F. K. L.; Sung, J. J. Y.; Kaplan, G. G. Worldwide incidence and prevalence of inflammatory bowel disease in the 21st century: a systematic review of population-based studies. *Lancet* **2017**, *390* (10114), 2769−2778.

(2) Saleh, M.; Trinchieri, G. Innate immune mechanisms of colitis and colitis-associated colorectal cancer. *Nat. Rev. Immunol.* **2011**, *11* (1), 9−20.

(3) Vieujean, S.; Jairath, V.; Peyrin-Biroulet, L.; Dubinsky, M.; Iacucci, M.; Magro, F.; Danese, S. Understanding the therapeutic toolkit for inflammatory bowel disease. *Nat. Rev. Gastro. Hepat.* **2025**, *22* (6), 371−394.

(4) Liu, J.; Di, B.; Xu, L.-l. Recent advances in the treatment of IBD: Targets, mechanisms and related therapies. *Cytokine Growth Factor Rev.* **2023**, *71*−*72*, 1−12.

(5) Ramos, G. P.; Papadakis, K. A. Mechanisms of disease: inflammatory bowel diseases. *Mayo Clin. Proc.* **2019**, *94* (1), 155−165.

(6) Khor, B.; Gardet, A.; Xavier, R. J. Genetics and pathogenesis of inflammatory bowel disease. *Nature* **2011**, *474* (7351), 307−17.

(7) Muro, P.; Zhang, L.; Li, S.; Zhao, Z.; Jin, T.; Mao, F.; Mao, Z. The emerging role of oxidative stress in inflammatory bowel disease. *Front. Endocrinol.* **2024**, *15*, No. 1390351.

(8) Zeng, Y.; Fan, M.; Zhou, Q.; Chen, D.; Jin, T.; Mu, Z.; Li, L.; Chen, J.; Qiu, D.; Zhang, Y.; Pan, Y.; Shen, X.; Cai, X. Reactive oxygen species-activated CO versatile nanomedicine with innate gut immune and microbiome remodeling effects for treating inflammatory bowel disease. *Adv. Funct. Mater.* **2023**, *33* (49), No. 2304381.

(9) Bhattacharyya, A.; Chattopadhyay, R.; Mitra, S.; Crowe, S. E. Oxidative stress: an essential factor in the pathogenesis of gastrointestinal mucosal diseases. *Physiol. Rev.* **2014**, *94* (2), 329−354.

(10) Nathan, C.; Cunningham-Bussel, A. Beyond oxidative stress: an immunologist's guide to reactive oxygen species. *Nat. Rev. Immunol* **2013**, *13* (5), 349−361.

(11) Li, Q.; Lin, L.; Zhang, C.; Zhang, H.; Ma, Y.; Qian, H.; Chen, X. L.; Wang, X. The progression of inorganic nanoparticles and natural products for inflammatory bowel disease. *J. Nanobiotechnol.* **2024**, *22* (1), 17.

(12) Tian, L.; Huang, J.; Xu, Y.; Zhao, P.; Li, Y.; Wei, X.; Li, M.; Jiang, S.; Huang, Q.; Xu, Y.; Lu, C.; Ding, J.; Zhou, W.; Gao, X. Dual-functional tea polyphenol−serotonin nanoparticles for integrated inflammation suppression and mucosal repair in inflammatory bowel disease. *Biomaterials* **2026**, *331*, No. 124076.

(13) Li, Z.; Yang, Q. Biomarker-responsive nanomaterials for precision theranostics in inflammatory bowel disease. *Coord. Chem. Rev.* **2026**, *552*, No. 217467.

(14) Zhang, Y.; Wang, T.; Sun, M.; Song, Y.; Huang, X.; Zhang, S.; Yang, J.; Zhang, J. Advanced nanomedicine: redefining therapeutic paradigms for inflammatory bowel disease. *Adv. Healthcare Mater.* **2023**, *12* (19), No. 2300069.

(15) Zhou, F.; Li, M.; Chen, M.; Chen, M.; Chen, X.; Luo, Z.; Cai, K.; Hu, Y. Redox homeostasis strategy for inflammatory macrophage reprogramming in rheumatoid arthritis based on ceria oxide nanozyme-complexed biopolymeric micelles. *ACS Nano* **2023**, *17* (5), 4358−4372.

(16) Gu, J.; Zhang, P.; Li, H.; Wang, Y.; Huang, Y.; Fan, L.; Ma, X.; Qian, X.; Xi, J. Cerium-luteolin nanocomplexes in managing inflammation-related diseases by antioxidant and immunoregulation. *ACS Nano* **2024**, *18* (8), 6229−6242.

(17) Cheng, H. P.; Bao, X. W.; Luo, Y. Y.; Li, Y. H.; Zhou, Y.; Hua, Q. Z.; Qiu, Y. J.; Liang, X. Y.; Huang, Y. H.; Liu, W.; Tang, S. Y.; Feng, D. D.; Li, C.; Luo, Z. Q. Sulfasalazine ameliorates lipopolysaccharide-induced acute lung injury by inhibiting oxidative stress and nuclear factor-kappaB pathways. *Int. J. Biochem. Cell Biol.* **2024**, *169*, No. 106530.

(18) Zheng, H.; Chen, M.; Li, Y.; Wang, Y.; Wei, L.; Liao, Z.; Wang, M.; Ma, F.; Liao, Q.; Xie, Z. Modulation of gut microbiome composition and function in experimental colitis treated with sulfasalazine. *Front. Microbiol.* **2017**, *8*, 1703.

(19) Huang, Y.; Xu, J.; Sun, G.; Cheng, X.; An, Y.; Yao, X.; Nie, G.; Zhang, Y. Enteric-coated cerium dioxide nanoparticles for effective inflammatory bowel disease treatment by regulating the redox balance and gut microbiome. *Biomaterials* **2025**, *314*, No. 122822.

(20) Wirtz, S.; Popp, V.; Kindermann, M.; Gerlach, K.; Weigmann, B.; Fichtner-Feigl, S.; Neurath, M. F. Chemically induced mouse models of acute and chronic intestinal inflammation. *Nat. Protoc.* **2017**, *12* (7), 1295−1309.

(21) Zhou, C.; Xia, Y.; Wei, Y.; Cheng, L.; Wei, J.; Guo, B.; Meng, F.; Cao, S.; van Hest, J. C. M.; Zhong, Z. GE11 peptide-installed chimaeric polymersomes tailor-made for high-efficiency EGFR-targeted protein therapy of orthotopic hepatocellular carcinoma. *Acta Biomater.* **2020**, *113*, 512−521.

(22) Yang, C.; Liu, W.; Liu, H.; Fan, T.; Tan, T.; Feng, Q.; Wang, W.; Tang, Z.; Li, G. Dynamic Intermediate Coordination on Cerium Dual Sites in MOFs Boosts Selective Epoxidation of Alkenes. *Adv. Mater.* **2026**, *38* (24), No. e72948.

(23) Zheng, J.; Chen, J.; Zhang, W.; Wu, Y.; Qin, T.; Fa, Y.; Dong, Q.; Zhang, R.; Qiu, Y. Tryptophan attenuates acute hypoxic stress-induced intestinal injury through the modulation of intestinal barrier integrity and gut microbiota homeostasis. *Genes Dis.* **2025**, *12* (6), No. 101627.

(24) Low, J. T.; Kim, Y.; Matsushita, M.; Ho, P.-C. Role of oxygen sensing and hypoxia-inducible factors in orchestrating innate immune responses. *Nat. Immunol.* **2025**, *26* (12), 2138−2147.

(25) Biasi, F.; Leonarduzzi, G.; Oteiza, P. I.; Poli, G. Inflammatory bowel disease: mechanisms, redox considerations, and therapeutic targets. *Antioxid. Redox Signal.* **2013**, *19* (14), 1711−47.

(26) Pacher, P.; Beckman, J. S.; Liaudet, L. Nitric oxide and peroxynitrite in health and disease. *Physiol. Rev.* **2007**, *87* (1), 315−424.

(27) Radi, R. Peroxynitrite, a stealthy biological oxidant. *J. Biol. Chem.* **2013**, *288* (37), 26464−72.

(28) Fang, H.; Sha, Y.; Yang, L.; Jiang, J.; Yin, L.; Li, J.; Li, B.; Klumperman, B.; Zhong, Z.; Meng, F. Macrophage-targeted hydroxychloroquine nanotherapeutics for rheumatoid arthritis therapy. *ACS Appl. Mater. Interfaces* **2022**, *14* (7), 8824−8837.

(29) Na, Y. R.; Stakenborg, M.; Seok, S. H.; Matteoli, G. Macrophages in intestinal inflammation and resolution: a potential therapeutic target in IBD. *Nat. Rev. Gastroenterol. Hepatol.* **2019**, *16* (9), 531−543.

(30) Hegarty, L. M.; Jones, G.-R.; Bain, C. C. Macrophages in intestinal homeostasis and inflammatory bowel disease. *Nat. Rev. Gastroenterol. Hepatol.* **2023**, *20* (8), 538−553.

(31) Cao, J.; Sha, Y.; Sun, M.; Yang, L.; Lv, R.; Cao, L.; Zhong, Z.; Meng, F. Sustained codelivery of heat shock protein peptide and rapamycin via nano-in-hydrogel induces immune tolerance in rheumatoid arthritis. *J. Controlled Release* **2025**, *383*, No. 113842.

(32) Tao, S.; Song, M.; Fan, J.; Zhu, F.; Lv, T.; Wei, H. Lactobacillus johnsonii-derived extracellular vesicles carrying GAPDH protect against ulcerative colitis through modulating macrophage polarization. *J. Adv. Res.* **2026**, *81*, 409−424.

(33) Rivera, C. A.; Randrian, V.; Richer, W.; Gerber-Ferder, Y.; Delgado, M.-G.; Chikina, A. S.; Frede, A.; Sorini, C.; Maurin, M.; Kammoun-Chaari, H.; Parigi, S. M.; Goudot, C.; Cabeza-Cabrerizo, M.; Baulande, S.; Lameiras, S.; Guermonprez, P.; Reis e Sousa, C.; Lecuit, M.; Moreau, H. D.; Helft, J.; Vignjevic, D. M.; Villablanca, E. J.; Lennon-Duménil, A.-M. Epithelial colonization by gut dendritic cells promotes their functional diversification. *Immunity* **2022**, *55* (1), 129−144.
(34) Nikolakis, D.; de Voogd, F. A. E.; Pruijt, M. J.; Grootjans, J.; van de Sande, M. G.; D'Haens, G. R. The role of the lymphatic system in the pathogenesis and treatment of inflammatory bowel disease. *Int. J. Mol. Sci.* **2022**, *23* (3), 1854.
(35) Wei, K.; Xu, Y.; Nie, C.; Wei, Q.; Xie, P.; Chen, T.; Jiang, J.; Chu, X. A Multifunctional Peptide Nucleic Acid/Peptide Copolymer-Based Dual-Mode Biosensor with Macrophage-Hitchhiking for Enhanced Tumor Imaging and Urinalysis. *J. Am. Chem. Soc.* **2024**, *146* (48), 33075−33083.
(36) Wang, X.; Liu, Y.; Fan, Y.; Yan, J.; Yan, G.; Liu, Q.; Xu, Q.; Wang, L.; Pan, D.; Xu, Y.; Chen, C.; Chen, Y.; Yang, M. Imaging Identifies Superior Inflammation Targeting of M1Macrophages for Cryo-Shocked Cell Pulmonary Drug Delivery to Treat Acute Lung Injury. *Adv. Healthcare Mater.* **2024**, *13* (30), No. 2401685.
(37) Yue, L.; Gao, C.; Li, J.; Chen, H.; Lee, S. M. Y.; Luo, R.; Wang, R. Chemotaxis-guided Self-propelled Macrophage Motor for Targeted Treatment of Acute Pneumonia. *Adv. Mater.* **2023**, *35* (20), No. 2211626.
(38) Dolinger, M.; Torres, J.; Vermeire, S. Crohn's disease. *Lancet* **2024**, *403* (10432), 1177−1191.
(39) Katsandegwaza, B.; Horsnell, W.; Smith, K. Inflammatory Bowel Disease: A Review of Pre-Clinical Murine Models of Human Disease. *Int. J. Mol. Sci.* **2022**, *23* (16), 9344.
(40) Roda, G.; Chien Ng, S.; Kotze, P. G.; Argollo, M.; Panaccione, R.; Spinelli, A.; Kaser, A.; Peyrin-Biroulet, L.; Danese, S. Crohn's disease. *Nat. Rev. Dis. Primers* **2020**, *6* (1), 22.
(41) Desreumaux, P.; Foussat, A.; Allez, M.; Beaugerie, L.; Hébuterne, X.; Bouhnik, Y.; Nachury, M.; Brun, V.; Bastian, H.; Belmonte, N.; Ticchioni, M.; Duchange, A.; Morel−Mandrino, P.; Neveu, V.; Clerget−Chossat, N.; Forte, M.; Colombel, J. F. Safety and efficacy of antigen-specific regulatory T-Cell therapy for patients with refractory Crohn's disease. *Gastroenterology* **2012**, *143* (5), 1207−1217.e2.
(42) Arbore, G.; West, E. E.; Spolski, R.; Robertson, A. A. B.; Klos, A.; Rheinheimer, C.; Dutow, P.; Woodruff, T. M.; Yu, Z. X.; O'Neill, L. A.; Coll, R. C.; Sher, A.; Leonard, W. J.; Köhl, J.; Monk, P.; Cooper, M. A.; Arno, M.; Afzali, B.; Lachmann, H. J.; Cope, A. P.; Mayer-Barber, K. D.; Kemper, C. T helper 1 immunity requires complement-driven NLRP3 inflammasome activity in CD4+ T cells. *Science* **2016**, *352* (6292), No. aad1210.

https://doi.org/10.1021/acs.biomac.6c00702
Biomacromolecules 2026, 27, 4734−4746